Monthly Notices
of the
ROYAL ASTRONOMICAL SOCIETY

MNRAS **494,** 1681–1692 (2020)
Advance Access publication 2020 March 24

doi:10.1093/mnras/staa800

Deep spectroscopy in nearby galaxy clusters – V. The Perseus cluster

J. A. L. Aguerri [1,2]★ M. Girardi,[3,4]★ I. Agulli,[1,2] A. Negri [1,2] C. Dalla Vecchia [1,2] and L. Domínguez Palmero[1,5]

[1]*Instituto de Astrofísica de Canarias, C/ Vía Láctea s/n, E-38205 La Laguna, Spain*
[2]*Departamento de Astrofísica, Universidad de La Laguna, E-38200 La Laguna, Tenerife, Spain*
[3]*Dipartimento di Fisica-Sezione Astronomia, Università di Trieste, via Tiepolo 11, I-34143 Trieste, Italy*
[4]*INAF-Osservatorio Astronomico di Trieste, via Tiepolo 11, I-34143 Trieste, Italy*
[5]*Isaac Newton Group of Telescopes, Apartado 321, E-38700 Santa Cruz de La Palma, Canary Islands, Spain*

Accepted 2020 March 17. Received 2020 January 23; in original form 2019 July 5

ABSTRACT

Dwarfs are the largest population of galaxies in number in the nearby Universe. Deep spectroscopic data are still missing to obtain a better understanding of their formation and evolution processes. This study shows the results obtained from a spectroscopic campaign in the Perseus cluster. We have obtained 963 new galaxy spectra. We have measured the recessional velocity of the galaxies by using a cross-correlation technique. These data have been used to obtain the cluster membership, the dynamics of the galaxies, and the spectroscopic luminosity function (LF) of the cluster. The cluster membership was obtained by using the peak + gap technique, reporting a total of 403 galaxies as cluster members within $1.4r_{200}$. The mean velocity and velocity dispersion of the cluster galaxies are $V_c = 5258$ km s^{-1} and $\sigma_c = 1040$ km s^{-1}, respectively. We obtained $M_{200} = 1.2 \times 10^{15}$ M$_\odot$ and $r_{200} = 2.2$ Mpc for this cluster. The clusters members were classified blue and red according to their $g - r$ stellar colour. The velocity dispersion of these two families of galaxies is different, indicating that the blue galaxies can be classified as recently accreted into the cluster. We present the spectroscopic galaxy LF of the cluster. This function turned to be flat: $\alpha = 0.99 \pm 0.06$. In addition, blue and red galaxies show similar densities in the faint end of the LF. This indicates that Perseus does not have a population of red dwarf galaxias as large as other nearby clusters. We have compared the LF of the Perseus cluster with other spectroscopic LFs of nearby clusters and those from cosmological simulations. This comparison shows that the spectroscopic LF of nearby galaxy cluster is far from universal.

Key words: galaxies: clusters: general – galaxies: clusters: individual: Abell 426.

1 INTRODUCTION

During the last two decades, large-area spectroscopic surveys have been powerful tools for the understanding of the evolution of the galaxies in nearby clusters. We can mention surveys such as ENACS (Katgert et al. 1996), 2dF cluster survey (De Propris et al. 2002), Sloan Digital Sky Survey (SDSS; Zandivarez & Martínez 2011), or WINGS (Fasano et al. 2006), which have provided valuable information about the properties of the galaxy population from clusters to group of galaxies and from the cluster centre to several virial radii. Medium redshift cluster surveys like CLASH (Postman et al. 2012) and eDISC (White et al. 2005) have also provided information about the role played by the environment in the evolution of the properties of galaxies in the last 5–6 Gyr. All these surveys are focused on the bright galaxy population. The properties of the dwarf galaxy population (the largest in number in the nearby Universe) are only analysed in few nearby environments such as the Virgo cluster (see Lisker et al. 2006a; Lisker, Grebel & Binggeli 2006b; Toloba et al. 2009), the Coma cluster (see Aguerri et al. 2005; Smith, Lucey & Hudson 2009), the Fornax cluster (see Iodice et al. 2016), or few nearby groups (see Tully 1988). Deep spectroscopic surveys down to the dwarf luminosity regime ($\sim M_r^* + 6$) for a large sample of nearby galaxy clusters remain to be done. This type of surveys will provide us information about the properties of the low-mass galaxy population in high-density environments, which is still poorly understood. These data would also provide a local milestone for other next-generation high-redshift surveys such as Euclid (Laureijs et al. 2011), J-PAS (Benitez et al. 2014), J-PLUS (Cenarro et al. 2019), or LSST (Ivezić et al. 2019).

Dwarf galaxies ($M_B > -18.0$) are the largest population of galaxies in number in the nearby Universe (Phillipps et al. 1998).

★ E-mail: jalfonso@iac.es (JALA); marisa.girardi@inaf.it (MG)

Their properties strongly depend on the local environment where they live. In particular, red dwarf galaxies, usually called dwarf ellipticals (dE), are mainly located in high-density environments. In contrast, blue dwarf galaxies are preferentially found in low-density environments (Sánchez-Janssen, Aguerri & Muñoz-Tuñón 2008). In addition, dwarf galaxies present a variety of morphologies linked with the environment (Lisker et al. 2006a, b, 2007). The different properties of dwarf galaxies in clusters and in the field have been extensively used in order to link the origin and evolution of low-mass galaxies and the local environment (see Boselli & Gavazzi 2014, for a review). The number of dwarf satellites in haloes of different masses has important cosmological implications. Thus, the total number of dwarf galaxies is much lower than expected from models. This is the well-known missing satellite problem presented from Milky Way mass haloes to cluster ones, and is one of the main problems associated with current galaxy formation theories (see e.g. Silk & Mamon 2012).

From the theoretical point of view, galaxies in clusters can be transformed according to several physical mechanisms such as tidal interactions between galaxies and the cluster potential (Mihos & Hernquist 1994; Mastropietro et al. 2005; Aguerri & González-García 2009); gas stripping (Gunn & Gott 1972; Quilis, Moore & Bower 2000); strangulation (Larson, Tinsley & Caldwell 1980; Peng, Maiolino & Cochrane 2015); and starvation (Balogh, Navarro & Morris 2000; van de Voort et al. 2017). These processes can produce strong transformations in the galaxy morphology (Moore, Lake & Katz 1998; Aguerri, Balcells & Peletier 2001; Aguerri et al. 2004; Lisker et al. 2006b), kinematics (Pedraz et al. 2002; Geha, Guhathakurta & van der Marel 2003; Toloba et al. 2009), and stellar populations (Haines et al. 2006; Smith et al. 2009). These physical mechanisms can sweep out part of the stellar and/or gas content of galaxies and form the so-called intracluster light observed in several nearby clusters (Arnaboldi et al. 2002; Aguerri et al. 2005; Mihos et al. 2005; Castro-Rodriguéz et al. 2009).

The low mass of dwarf galaxies makes them ideal targets to be transformed by these physical processes active in high-density environments. Several observational properties of dwarf galaxies in nearby clusters point towards the fact that they are products of strongly transformed galaxies by the environment. We can mention the structural parameters observed in some dEs and dwarf S0 galaxies (Aguerri 2016), the presence of more fast rotators in dwarfs located in the external regions of the clusters (Toloba et al. 2015), or the recent quench of the star formation for some of the dwarf galaxies in nearby clusters (Paccagnella et al. 2017; Aguerri, Agulli & Méndez-Abreu 2018). Nevertheless, these results are based on few nearby galaxy clusters and a study on the properties of dwarf galaxies in a large cluster sample remains to be done. Indeed, the different time-scale of these mechanisms and their different action regions in clusters make it difficult to know what is the main physical mechanism driving the evolution of galaxies (Treu et al. 2003).

We have started a programme to obtain deep spectroscopy in a sample of nearby galaxy clusters to analyse the origin and evolution of their dwarf population. This project has analysed so far the dynamical and photometric properties of the dwarf population in two nearby clusters: A 85 (Agulli et al. 2014, 2016a; Yu et al. 2016; Aguerri et al. 2017, 2018) and A 2151 (the Hercules cluster; Agulli et al. 2016b, 2017). The programme will continue in the near future by using the large multiplexing of the new spectrograph called WEAVE planned for the William Herschel Telescope (WHT; Dalton et al. 2012).

One of the goals of this project is to study the spectroscopic luminosity functions (LFs) of the galaxies in nearby clusters. The LF of galaxies is a simple statistic that tell us about the density of objects located within a given volume of space as a function of the magnitude. The comparison of the LFs of different environments can tell about the evolution of the galaxy populations with the galaxy density. The LF of galaxies in clusters has been extensively studied by using photometric data. These studies have shown that in general both the bright and faint ends of the LF are different in the field and clusters. In particular, the slope of the faint end of the LF is much steeper in clusters than in field (see e.g. Popesso et al. 2006). This points to a more abundant dwarf galaxy population in high-density environments than in the field (Zandivarez & Martínez 2011). The spectroscopic confirmation of this result has been treated by few studies on individual clusters with uncertain results (Rines & Diaferio 2006; Agulli et al. 2014, 2016b).

This paper is focused on the Perseus cluster (Abell 426) and is the fifth of a series of papers to study the properties of the dwarf galaxy population in nearby galaxy clusters. The paper is organized as follows. Section 2 shows the data and the procedure followed for obtaining the recessional velocities of the galaxies and the cluster membership. Section 3 show the results. The discussion and conclusions are given in Sections 4 and 5. Through this paper, we have used the cosmology given by $\Omega_\Lambda = 0.7$, $\Omega_m = 0.3$, and $H_0 = 70$ Mpc^{-1} km s^{-1}.

2 SPECTROSCOPIC DATA OF THE PERSEUS CLUSTER

2.1 The Perseus cluster

The Perseus cluster (A 426) is one of the most massive galaxy aggregations of the nearby Universe. It is classified as a Bautz–Morgan type II–III cluster, of richness class 2. This cluster belongs to the Perseus-Pisces supercluster, which is one of the two dominant concentrations of galaxies in the nearby Universe. In particular, this supercluster is located at a recessional velocity of $4500 < V < 5500$ km s^{-1} (Giovanelli & Haynes 1985; Wegner, Haynes & Giovanelli 1993; Hudson et al. 1997).

A massive cD galaxy (NGC 1275) is visible at the cluster centre ($\alpha(J2000) = 3^h19^m46^s.9$; $\delta(J2000) = 41°30'48''$). Struble & Rood (1999), using recessional velocities of 192 galaxies members, reported that the redshift of the cluster was $z_c = 0.0167$ and its velocity dispersion $\sigma_c = 1324$ km s^{-1}. A strong spatial segregation of galaxy morphologies was observed in this cluster (Andreon 1994). This could indicate that this cluster is dynamically unrelaxed.

At X-ray wavelengths, Perseus shows the highest X-ray temperature in the sky. The shape of the X-ray emission is not round, and presents an elongated shape towards the west of the cluster (see e.g. Ettori, Fabian & White 1998). In addition, X-ray substructure has been measured in this cluster (Mohr, Fabricant & Geller 1993). The two-dimensional temperature map of the cluster presents substructure that has been interpreted as the consequence of several recent mergers of other clusters or groups (see Schwarz et al. 1992; Ettori et al. 1998; Furusho et al. 2001).

The mass and r_{200} reported from X-ray observations are $M_{200} = 6.65 \times 10^{14}$ M$_\odot$ and $r_{200} = 1.79$ Mpc (Simionescu et al. 2011). This mass is smaller than that of Coma cluster. However, the core of the Perseus cluster reaches a density similar to that on the Coma cluster. The similar distributions of low surface brightness galaxies in the central regions of Coma and Perseus confirm the similar density at the core of the two clusters (Weinmann et al. 2011; Wittmann et al. 2017).

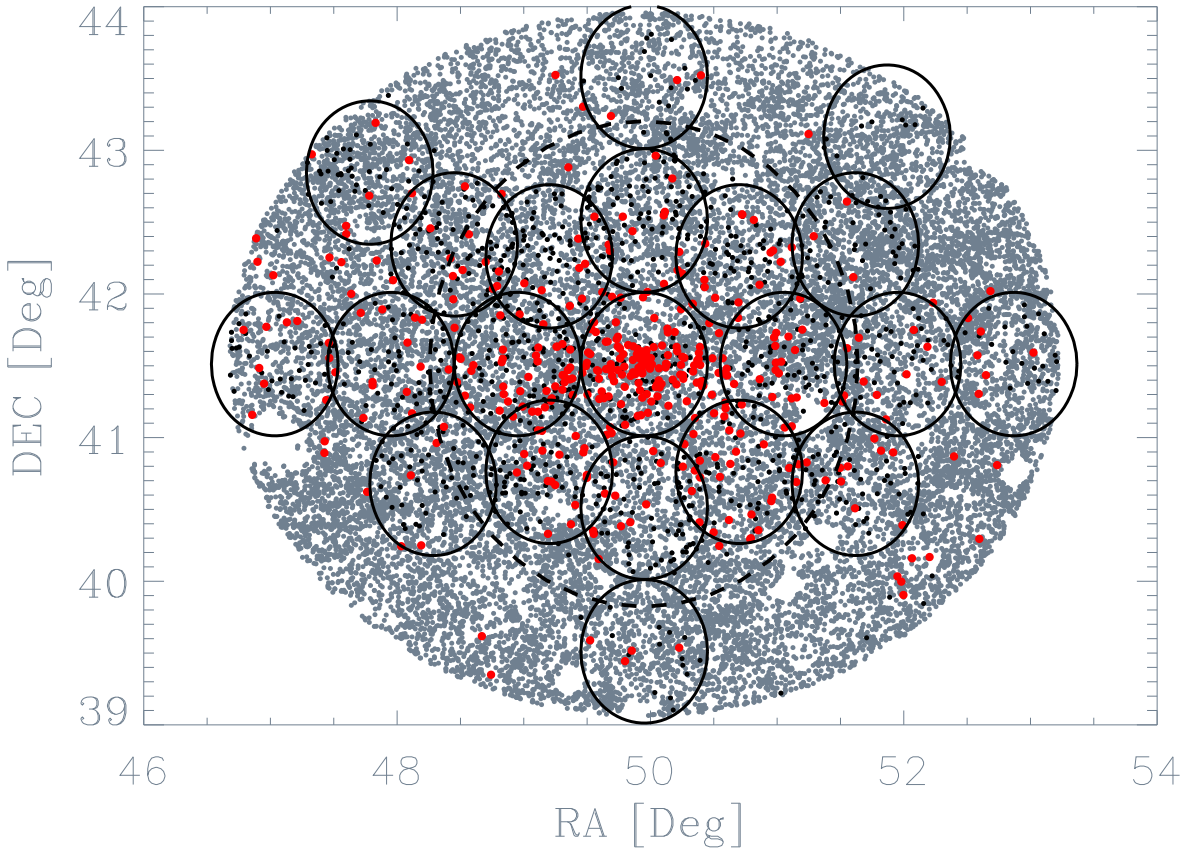

Figure 1. Sky position of the galaxies in the photometric catalogue (grey points), and spectroscopic targets resulting in non-cluster members (black points) and cluster members (red points). The circles with full line represent the AF2 pointings. The dashed line represents a circle with radius equal to r_{200}.

2.2 Spectroscopic data of the cluster

We run an observational campaign to obtain massive and deep spectroscopy of the galaxies in the direction of the Perseus cluster. The target galaxies for the spectroscopic observations were selected from the SDSS Data Release 10 (SDSS-DR10; Ahn et al. 2014). The photometric catalogue was made by all objects classified as galaxies at the SDSS-DR10 data base within a radius of 147 arcmin (3.0 Mpc at the cluster distance) around the centre of the cluster, considered at the position of the cD galaxy.

The spectroscopic targets were selected among the photometric objects with three additional constraints: (i) no recessional velocity available; (ii) bluer than $g - r = 1.0$; and (iii) brighter than $m_r = 20.0$. The colour constraint was used in order to avoid background objects. In addition, the apparent magnitude limit was considered due to the properties of the spectrograph used for the observations. Photometric and spectroscopic targets are shown in Fig. 1.

The spectroscopic observations were carried out by using the fibre spectrograph AutoFiber2/WYFFOS at the WHT during a run of four nights in 2015 November. We observed a total of 21 different pointings within 147 arcmin from the cluster centre (see Fig. 1). We collected three exposures of 1800 s per pointing to reach a signal-to-noise ratio (S/N) higher than 5 for the faintest galaxies of the sample. The instrumental configuration employs the grism R158B, which has a resolution of $R \approx 280$ at the central wavelength $\lambda \approx 4500$ Å. A total of 1734 targets were observed.

The data reduction was carried out by using the instrument pipeline (version 2.25; see Domínquez Palmero et al. 2014). The pipeline allows us to produce the standard reduction and the correction for the attenuation of each fibre, previously evaluated with observed dome flats.

2.3 Velocity catalogue

The recessional velocity of the observed galaxies was obtained by using the rvsao.xcsao IRAF task (Kurtz et al. 1992). This task cross-correlates a template spectrum library with that observed. In this study, we used the library of templates provided by Kennicutt (1992). We determined a total of 963 recessional velocities. The remaining 771 spectra do not reach enough S/N to perform the cross-correlation. The small S/N in some of the allocated fibres could be due to several reasons: (i) The transparency of the sky was not the same during the full run of the observations. In particular, we have poor seeing and transparency during one of the nights of the run. This has affected significantly four pointings. (ii) AF2 has problems of vignetting across its field of view. Thus, spectroscopic targets located at a radial distance from the centre of the pointing larger than 15 arcmin can be affected by this vignetting.

Our observational strategy was designed to repeat the observations of a small number of objects in different pointings, in order to determine the uncertainties on the recessional velocities. A total of 29 galaxies were distributed among the different pointings. The mean of the differences in the velocity measurements of these objects was 137 km s^{-1}. This was assumed as the typical uncertainty for the recessional velocities.

The velocity catalogue was completed with those galaxies with recessional velocities from SDSS-DR12 and NED data bases.

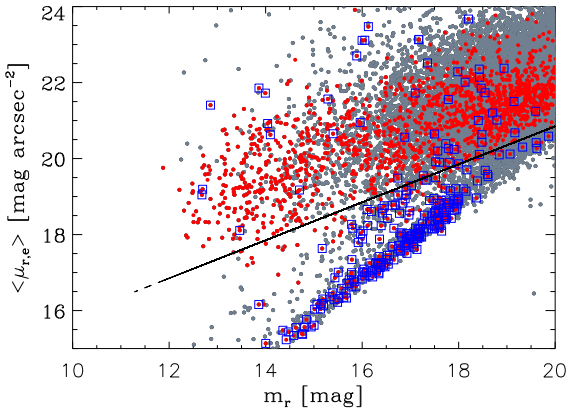

Figure 2. Mean effective surface brightness versus apparent *r*-band magnitude of the photometric targets (grey circles), galaxies with recessional measured velocity (red circles), and stars with recessional velocity (blue squares). The full line represents the separation between galaxies and stars. See text for more details.

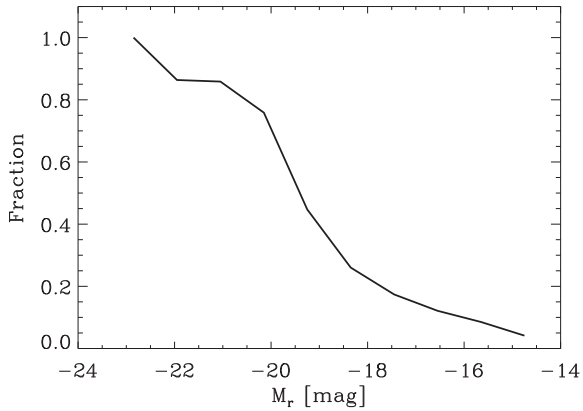

Figure 3. Fraction of galaxies with velocity measured as a function of the absolute magnitude in the *r* band. For the *x*-axis, we considered that all galaxies are at the cluster distance.

This makes a total of 1495 objects catalogued as galaxies by SDSS with recessional velocities. Fig. 2 shows mean effective radius ($\langle\mu_{r,e}\rangle$) and apparent magnitude (m_r) in the *r* band for the photometric targets and those objects with recessional velocities. Our observations reported recessional velocities for objects down to $m_r = 20.0$ and $\langle\mu_{r,e}\rangle \sim 22.0$ mag arcsec^{-2}.

Due to the low galactic latitude of the Perseus cluster, this region of the sky is contaminated by a large number of stars from our Galaxy. Although we have selected those objects classified as galaxies by SDSS, a fraction of them turned to be stars. In particular, 253 of our spectroscopic targets turned to have a recessional velocity smaller than 200 km s^{-1}. These stars represent 17 per cent of the total sample. We have represented the location of these stars in the $\langle\mu_{r,e}\rangle$–m_r plane (see Fig. 2). Note that most of the spectroscopically confirmed stars are located in a well-defined region of this diagram. The separation between galaxies and stars in Fig. 2 is clear down to $m_r \approx 18.0$. However, the separation is less evident for faint objects with $18 < m_r < 20$. We have defined a cut-off in order to remove stellar objects with no velocity information from our catalogues (see Fig. 2). This cut-off allows us to remove up to 81 per cent of the stars. In contrast, only 3 per cent of the galaxies are lost.

In addition to the galaxy–star separation proposed earlier, we have observed all individual objects brighter than $m_r = 20.0$ by using the SDSS images. Those objects with no recessional velocities and considered as stars after this visual inspection were removed from the photometric catalogue.

Fig. 3 shows the spectroscopic completeness (C) of our sample. C is defined as the ratio between the number of galaxies with measured velocities, N_z, and the number of photometric targets, $N_{\rm phot}$, per each magnitude bin. Fig. 3 shows that C is higher than 80 per cent for galaxies with $M_r < -20.0$. For fainter objects, C decreases being $\approx$10 per cent for galaxies with $M_r = -16.0$.

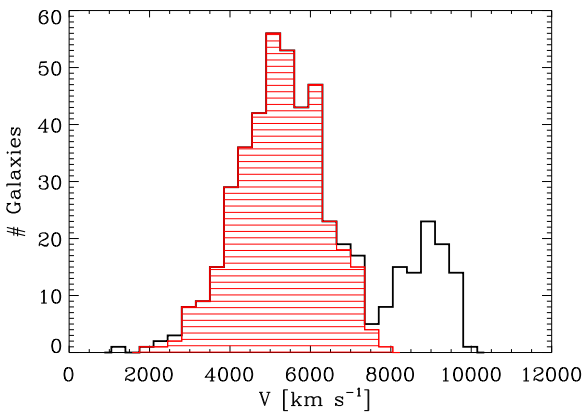

Figure 4. Velocity distribution of the galaxies in the direction of the Perseus cluster. The red histogram represents the velocity distribution of the galaxies selected as cluster members.

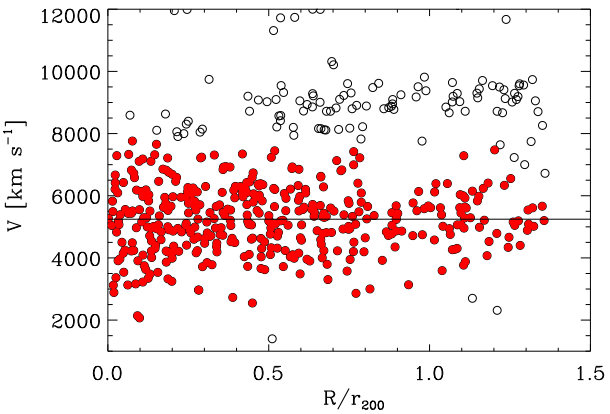

Figure 5. Radial velocity versus distance to the cluster centre. The red filled points represent the galaxies selected as cluster members. The open black circles correspond to non-member galaxies. The horizontal full line shows the recessional velocity of the cluster.

2.4 Cluster membership

Fig. 4 shows the velocity histogram of the galaxies with $V <$ 12000 km s^{-1} in the direction of the Perseus cluster. The histogram shows a bimodal distribution. One peak of the distribution is located at $V \approx$ 5000 km s^{-1} and corresponds to the Perseus recessional velocity. The other peak at $V \approx$ 9000 km s^{-1} corresponds to another group of galaxies. The non-isolation of the Perseus cluster is also observed in the caustic diagram (see Fig. 5).

The cluster membership was done by using the two-step method called peak + gap (Girardi et al. 2015). This method is a combination of the 1D-DEDICA (Pisani 1993), which is an adaptive

Table 1. Dynamical parameters of the galaxies in the Perseus cluster.

	N_{gal}	$\langle V_c \rangle$ (km s^{-1})	σ_c (km s^{-1})
All	403	5258	1040
Bright	319	5286	980
Dwarf	84	5049	1265
Red	332	5268	959
Blue	71	5139	1398

kernel method for the evaluation of the density probability function underlying a discrete data set, and the shifting gapper method, which uses both position and velocity information (Fadda et al. 1996). According to the DEDICA procedure, a total of 403 galaxies from our catalogue belong to the Perseus cluster. Their velocity distribution and location in the caustic diagram can be seen in Figs 4 and 5, respectively. This number of cluster members increases by a factor of 2 the value obtained from the literature.

3 PROPERTIES OF THE GALAXY POPULATION IN PERSEUS

We present in this section the properties of the galaxy population in the Perseus cluster. The results will be compared with those obtained from our group for the A 2151 and A 85 clusters (see Agulli et al. 2014, 2016a, b, 2017; Aguerri et al. 2017, 2018).

3.1 Dynamical parameters of the cluster

With the 403 cluster members, we have obtained that the mean velocity (V_c) and velocity dispersion (σ_c) of the cluster galaxies in Perseus are 5258 ± 52 and 1040^{+34}_{-43} km s^{-1}, respectively. Our value of velocity dispersion well agrees with the previous estimate (Girardi et al. 1998). Using the theoretical relation between mass and velocity dispersion of Munari et al. (2013) calibrated on simulated clusters, we have estimated the cluster mass $M_{200}(<r_{200} = 2.2$ Mpc$) = 1.2 \times 10^{15}$ M$_\odot$, with related uncertainties of 4 and 12 per cent on r_{200} and M_{200}, as propagated from the error on σ_c. An additional 10 per cent of uncertainty on mass is indicated by the scatter around the theoretical relation. Our values for r_{200} and M_{200} are about 1.2 and 1.8 larger than those obtained from X-ray measurements (see Simionescu et al. 2011).

We have divided the galaxies in the Perseus cluster according to their $g - r$ stellar colour and r-band luminosity. Thus, we have called bright and dwarf galaxies those brighter and fainter than $M_r = -18.0$, respectively. In addition, we have divided the galaxies into blue and red according to their position in the colour–magnitude diagram (see Sections 3.2 and 3.3). Table 1 shows the mean recessional velocity and dispersion velocity of the different families of galaxies considered in this study. The table shows that dwarf and blue galaxies have larger dispersion velocity than bright and red ones. In particular, the velocity dispersion of blue and dwarf galaxies is about $\sqrt{2}$ larger than that from red and bright ones. This has been observed in other samples of galaxies in clusters (see e.g. Sánchez-Janssen et al. 2008) and it has been interpreted that blue and dwarf galaxies are less dynamically relaxed objects than red and bright ones. In addition, it can also be interpreted that blue and dwarf galaxies are located in more radial orbits than red and bright ones (see Aguerri et al. 2017).

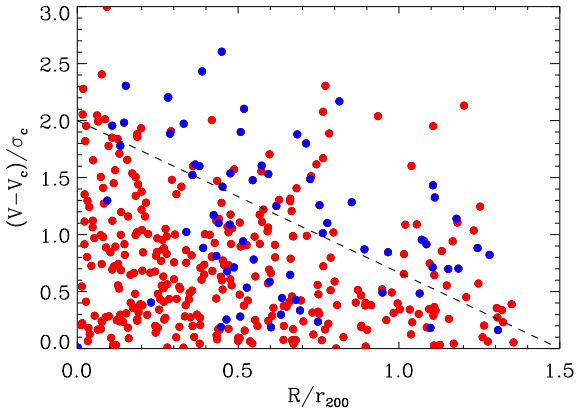

Figure 6. Rest-frame and normalized radial velocity versus distance from the cluster centre. The red filled points represent the galaxies selected as cluster members. The open black circles correspond to non-member galaxies. The horizontal full line shows the recessional velocity of the cluster. The dashed line separates galaxies with infall time smaller and larger than 1 Gyr according to Oman et al. (2013).

The different dynamic state of the galaxy families can also be seen in the location of galaxies in the caustic plane (see Fig. 6). Only 40 per cent of the blue galaxies are located at cluster-centric distances smaller than $0.5r_{200}$. In addition, only 2/71 blue galaxies are located in the core cluster region defined by $R/r_{200} < 0.5$ and $(V - V_c)/\sigma_c < 1.0$.

Oman, Hudson & Behroozi (2013) showed that the position of the galaxies in the caustic diagram is related to their infall time into the cluster. They proposed a separation between galaxies with infall time shorter than 1 Gyr and those accreting into the cluster several Gyr ago. This separation is given by the line $|V - V_c|/\sigma_c = -(4/3)R/r_{200} + 2.0$. Fig. 6 shows this separation. We obtain that only 12 per cent of the cluster members can be classified as recently accreted. We have also obtained that about 60 per cent of the blue galaxies can be considered as recent arrivals to the cluster. In contrast, only 8 per cent of the red galaxies are located in the caustic region corresponding to recent arrivals (see Fig. 6). These numbers obtained are different from the computed ones for A 85 and A 2151. For these clusters, about 30 per cent of the cluster members can be considered as recent arrivals (Agulli et al. 2016a, 2017). This is almost a factor of 2 larger than the recent arrivals observed in A 426. These results indicate that the present accretion rate of galaxies in A 426 is smaller than that of other nearby clusters.

3.2 Colour–magnitude diagram

Fig. 7 shows the colour–magnitude diagram of the galaxies in the Perseus cluster. A well-defined red sequence can be observed in this diagram. However, the red sequence is less defined for galaxies with $M_r > -19.0$. This dilution of the red sequence at faint magnitude has been observed in other nearby clusters such as the Hercules cluster (see Agulli et al. 2017). In contrast, other systems such as Abell 85 do not show this, and a well-defined red sequence can be observed down to the dwarf regime (see Agulli et al. 2014). The lack of red low-luminosity galaxies is not an observational bias. Recessional velocities of red low-luminosity galaxies have been measured resulting in non-member galaxies (see Fig. 7). This lack of red dwarf galaxies is in agreement with the results shown by Weinmann et al. (2011). In particular, they obtained that the

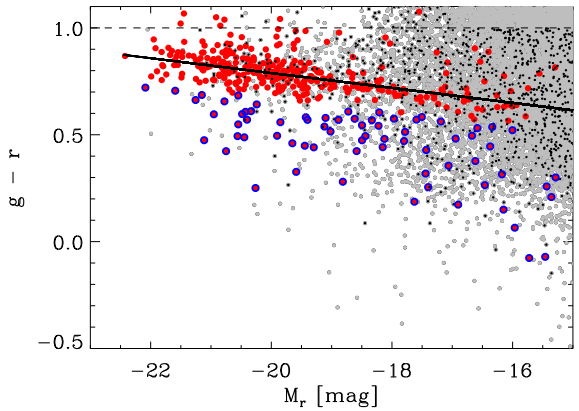

Figure 7. Colour–magnitude diagram of the galaxies in the direction of the Perseus cluster (grey points). Red filled and blue open circles represent the red and blue member galaxies, respectively. The black points show those galaxies with radial velocity but non-cluster members. The full black line is the fitted red sequence of the cluster. The dashed grey line shows the $g - r$ colour cut used for the target selection.

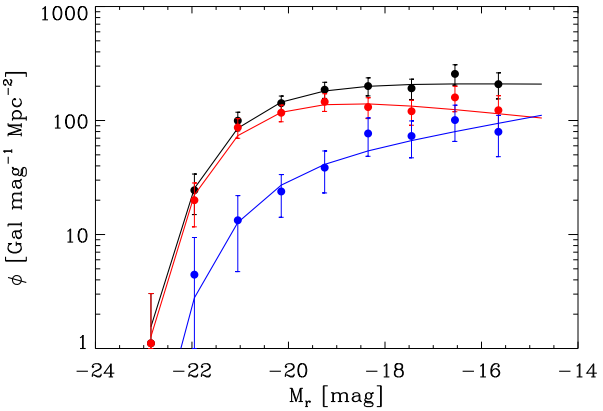

Figure 8. The black, red, and blue points show the spectroscopic LFs of all, red, and blue galaxies of the Perseus cluster. The lines represent the Schechter fits of the different LFs.

fraction of red galaxies in the Perseus cluster decreases at fainter magnitudes. Indeed, the fraction of red galaxies at $M_r > -18.0$ was smaller than that predicted by semi-analytical models of galaxy formation for this cluster.

The red sequence of the Perseus cluster shows also another peculiarity in its bright part. In fact, the $g - r$ colour dispersion (rms) of the red sequence of the cluster for galaxies with $M_r < -19.0$ is 0.06, which is about two times larger than the rms values of other clusters such as Hercules or Abell 85.

3.3 The spectroscopic luminosity function of the cluster

The LF is an observable that gives us the luminosity distribution of satellite galaxies in our system. While it has been extensively analysed in clusters (e.g. Popesso et al. 2006; Zandivarez & Martínez 2011) and field (e.g. Blanton et al. 2003) using photometric data, very few clusters have been analysed down to the dwarf regime by using spectroscopy (Mobasher et al. 2003; Rines & Diaferio 2006; Agulli et al. 2014, 2016a, 2017). Following the prescription from Agulli et al. (2014), we have computed the spectroscopic LF in the Perseus cluster, giving a certain binning of M_r values, with $\Delta M_r = 0.5$; the LF can be computed as

$$\Phi(M_r) = N_{\rm phot}(M_r) \times f_{\rm m}(M_r)/(\Delta M_r \times A), \quad (1)$$

where $N_{\rm phot}(M_r)$ is the number of photometric targets, $f_{\rm m}(M_r)$ is the fraction of cluster members, defined as the ratio between the number of cluster galaxies among those with measured velocity and the number of all galaxies with velocity ($N_{\rm vel}(M_r)$), and A is the surveyed area. Note that equation (1) can be rewritten by $\Phi(M_r) = N_{\rm m}/C$, where $N_{\rm m}$ is the number of cluster members and C is the spectroscopic completeness per magnitude bin. Fig. 8 represents the spectroscopic LF of the Perseus cluster down to $M_r = -16.0$. This figure also shows the spectroscopic LFs of the blue and red galaxy populations of the cluster.

We have fitted the LF of the cluster by a Schechter function (Schechter 1976). The LF of this cluster is well modelled by a single Schechter function, which has three free parameters: the normalization factor, ϕ^*, the characteristic luminosity of the cluster, M_r^*, and the slope of the faint end, α. In particular, the Schechter function has a power-law dependence at faint magnitudes and an exponential one at the bright end. M_r^* represents the magnitude at which the Schechter functions changes its dependence from an exponential to a power law. Table 2 shows the parameters of the Schechter function fitted for the total galaxy population of the cluster. Note the flatness of the LF of this cluster. In particular, $\alpha = -0.99 \pm 0.06$. The LF of the Perseus cluster does not show a faint upturn as in the case of A 85 (see Agulli et al. 2014).

Table 2. Parameters of the fitted Schechter functions.

Galaxy population	M_r^*	α
All	-21.11 ± 0.21	-0.99 ± 0.06
Red	-21.05 ± 0.22	-0.89 ± 0.08
Blue	-20.99 ± 0.79	-1.19 ± 0.14

We have also computed the LFs of the blue and red galaxy populations of the cluster (see Fig. 8). The red and blue populations of galaxies were selected according to their $g - r$ colour. In particular, blue galaxies are those with $(g - r) < (g - r)_{\rm RS} - 3\sigma_{\rm RS}$, and red galaxies are the remaining ones, where $(g - r)_{\rm RS}$ is the colour of the red sequence of the cluster and $\sigma_{\rm RS}$ represents its dispersion. Fig. 8 shows that the red population dominates the galaxy density down to $M_r \approx -18.0$. At the faint end, the galaxy densities of the blue and red populations are similar. The parameters of the Schechter functions fitted to the blue and red populations are also listed in Table 2.

The fact that neither the red nor the blue populations dominate in number the faint end of the LF makes Perseus different from A 85 or A 2151. In fact, in these two clusters the low-luminosity galaxy population is clearly dominated by the blue galaxies (A 2151; Agulli et al. 2017) or the red galaxies (A 85; Agulli et al. 2016a).

3.4 The dwarf-to-giant ratio

The parameters of the Schechter function are correlated. To avoid this effect, other non-parametric quantities such as the dwarf-to-giant (D/G) ratio have been computed for the Perseus cluster. We have defined as dwarf galaxies those with $-18 < M_r < -16$. Giant or bright galaxies were considered those with $M_r < -18$. The D/G ratio was computed by integrating the spectroscopic LFs in the luminosity ranges of the dwarf and giant definitions. To avoid aperture corrections, we have computed the D/G of the clusters within r_{200}. We obtained for A 426 a D/G $= 0.61 \pm 0.11$. We have

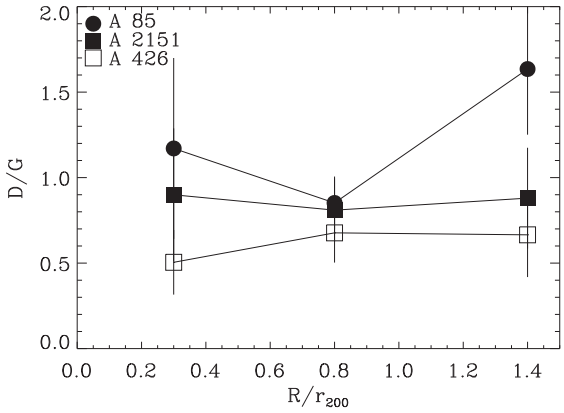

Figure 9. D/G ratio as a function of the cluster-centric distance for A 85 (full circles), A 2151 (full squares), and A 426 (open squares).

also computed the D/G ratio for the clusters A 85 and A 2151 by using their spectroscopic LFs (Agulli et al. 2014, 2016a). The D/G values obtained are 0.98 ± 0.14 and 0.78 ± 0.14 for A 85 and A 2151, respectively. The D/G ratio of the Perseus cluster is similar, within the uncertainties, to the value from A 2151. However, the D/G value of the Perseus cluster is significantly smaller than that obtained for A 85.

We have computed the variation of the D/G ratio as a function of the cluster-centric radius. Fig. 9 shows the radial variation of the D/G ratio for A 85, A 2151, and A 426. Note that the D/G ratio of A 426 shows the smallest values at all radii. In contrast, A 85 shows the largest values of the D/G ratio in particular at large cluster-centric distances. A 2151 shows a constant D/G ratio as a function of radius, and A 426 has smaller values of D/G in the innermost region of the cluster.

The variation of the D/G ratio could be due to variation in the number of dwarf galaxies, giants, or both. To understand these variations, we have computed the radial dependence of the number density of dwarf and giant galaxies for the three clusters. Fig. 10 shows the radial variation of the number galaxy density for dwarfs and giants for A 85, A 2151, and A 426. Note that the galaxy densities of dwarfs and giants are similar at all radii for A 85 and A 2151. In contrast, A 426 shows smaller density of dwarf galaxies at all cluster-centric distances. Indeed, A 426 shows the smallest density of dwarf galaxies at all radii for the three clusters. The radial giant density is similar in A 85 and A 2151. In contrast, the giant number density is larger for A 426. The low density of dwarfs and the high density of giant galaxies are the reasons why A 426 shows the smallest D/G ratio among the three clusters.

4 DISCUSSION

4.1 Comparison between the photometric and spectroscopic LFs in the Perseus cluster

Photometric LFs of clusters show a larger population in number of dwarf galaxies than in the field. This is reflected in steep faint ends of the photometric LFs in clusters (see Popesso et al. 2006). However, the spectroscopic LFs measured so far in a limited number of nearby clusters do not agree with that. The measured spectroscopic LFs in clusters show flatter faint ends than the photometric ones and only in one cluster (A 85) show a clear upturn (see Rines & Diaferio 2006; Agulli et al. 2014, 2017). In this context, the spectroscopic LF of the Perseus cluster computed in this work is not different from other clusters. Spectroscopic observations of galaxies in clusters have always small spectroscopic completeness for low-luminosity galaxies. This lack of completeness can affect the measurements of the faint end of the spectroscopic LFs. This can be the case when the spectroscopic target galaxies do not represent the full galaxy population of the cluster. We avoid this in our study because the spectroscopic targets were selected randomly according to apparent magnitude and surface brightness cuts. This target selection avoids that a particular type of galaxies were primarily selected.

We have computed the photometric LF of the Perseus cluster to compare with the spectroscopic LF measured in this work. The photometric LF was computed by using a statistical subtraction of the background galaxies. To compute this galaxy background, we have selected 50 randomly distributed fields in the sky from SDSS-DR10 with the same aperture as the Perseus data. We computed the individual photometric LFs of these fields by selecting galaxies as we did for the Perseus cluster (see Sections 3.2 and 3.3). The individual LFs of the fields were combined to build a global background photometric LF, which was used for the statistical subtraction of the background of the photometric LF of the Perseus cluster. Fig. 11 shows the resulting photometric LF of the galaxies in the direction of the Perseus cluster. The total uncertainty of this

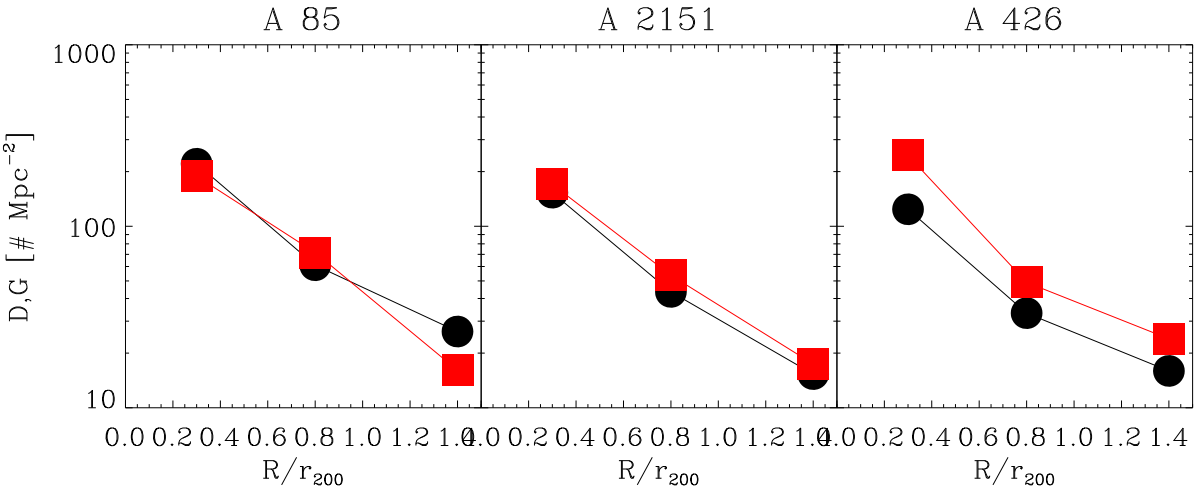

Figure 10. Radial variation of the galaxy density of dwarfs (full circles) and giants (red filled squares).

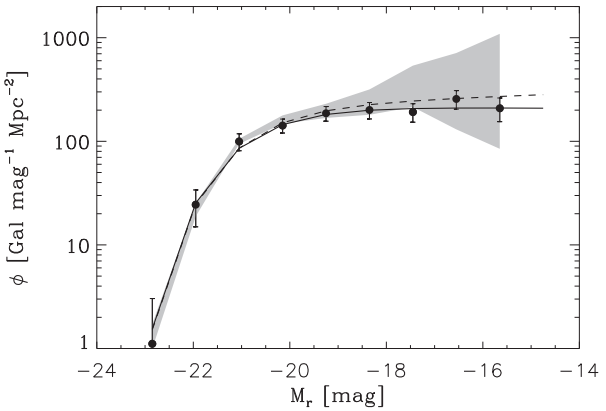

Figure 11. Photometric (shaded region) and spectroscopic (points) LFs of the Perseus cluster. The full and dashed lines show the best-fitting Schechter functions to the photometric and spectroscopic LFs, respectively.

LF was obtained by adding in quadrature the cosmic variation and the Poissonian uncertainties. The former is the larger term of these uncertainties. Note that the spectroscopic LF of the Perseus cluster is in agreement, within the uncertainties, with the photometric one. We have also fitted Schechter functions to the computed photometric LF. We obtained that one single Schechter function can fit the photometric LF. This indicates that the photometric LF of the Perseus cluster does not show an upturn, similarly to the spectroscopic one. Moreover, the fitted faint end of the photometric LF turned out to be $\alpha = -1.04 \pm 0.11$. This value is in agreement with a flat LF as that given by the spectroscopic one. These results indicate that the low spectroscopic completeness of our data at faint magnitudes does not affect the measurements of the faint end of the spectroscopic LF.

4.2 The bright and faint ends of the cluster LFs of nearby clusters

A large number of photometric LFs of nearby clusters can be found in the literature (see e.g. Popesso et al. 2006; Barkhouse, Yee & López-Cruz 2007; Lan, Ménard & Mo 2016). These LFs were computed by using photometric data and a statistical background subtraction. The photometric LF of the galaxies in the clusters is the galaxy number count excess after this statistical subtraction. Most of these photometric LFs report that nearby galaxy clusters show steeper faint ends than field galaxy LFs. In addition, the faint end of these LFs is dominated by red dwarf galaxies. These results indicate that red dwarf galaxies are basically located in high-density galaxy aggregations in the nearby Universe (Madgwick et al. 2002; Christlein & Zabludoff 2003; Popesso et al. 2006; Lan et al. 2016).

Few individual galaxy clusters have been observed with enough spectroscopic depth in order to obtain their LFs down to the dwarf regime ($M_r < -18.0$) and confirm the results obtained from photometric studies. We can mention the results on the clusters A 85 (Agulli et al. 2014, 2016a), Hercules (Agulli et al. 2017), A 2199 (Rines & Diaferio 2006), and the Perseus cluster shown in this work. This data set of clusters is small but is homogeneous in limiting magnitude ($M_r = -16.0$) and surveyed area ($R/R_{200} \sim 1.4$, except for A 2199) and makes it an ideal sample to compare their LF parameters. In addition to individual clusters, composite and deep spectroscopic LFs have been computed for a set of nearby clusters (De Propris et al. 2002; Christlein & Zabludoff 2003). These LFs are inhomogeneous, in surveyed area, magnitude depth, and observed filter. The parameters of the composite LFs should be taken as indicators of the mean LF parameters of the clusters.

Fig. 12 shows the M_r^* and α parameters of the spectroscopic LFs of the individual clusters and those from the composite samples. For comparison, we have also overplotted the parameter of the spectroscopic LF for the field (see Blanton et al. 2003). A common cosmology has been considered in this figure. In addition, we have transformed all data to the r band. We can see that for the different observed data sets of clusters there is a large variety of the LF parameters. The differences are larger for M_r^*. All observed cluster samples show spectroscopic LFs with $\alpha < 1.5$. Indeed, with the exception of A 85, the clusters show spectroscopic LFs with α between -1.0 and -1.3. These values are smaller than those obtained from photometric LF studies (see Popesso et al. 2006; Lan et al. 2016). In addition, these values of α are similar to the value of the field LF. This indicates that the number density of dwarf galaxies is similar in clusters and in the field. The differences in the values of M_r^* are larger. In particular, A 85 has the faintest M_r^* and the smallest α of the set of clusters. This value is similar to the M_r^* shown by the field LF. In contrast, Hercules, A 2199, and Perseus show LFs with brighter M_r^* and flatter faint ends. The Hercules cluster shows the LF with the brightest M_r^* value. The Perseus and A 2199 LFs show values of M_r^* between those from the Hercules and A 85 clusters. In addition to the individual clusters, Fig. 12 also shows LF parameters of the composite LF. We can see that they show values of M_r^* and α similar to A 2151. All these results suggest that the galaxy population of nearby galaxy clusters is not homogeneous, and the LF of nearby cluster is far from universal.

4.3 Comparison with simulations

Numerical simulations are powerful tools for the understanding of galaxy formation and evolution. The EAGLE simulation (Schaye et al. 2015) is one among the state-of-the-art hydrodynamical cosmological simulations currently available. EAGLE reproduces a volume of 100 co-moving Mpc on a side, and due to low statistics, objects such as large galaxy clusters are not present. We thus adopt the Cluster-EAGLE simulation (Bahé et al. 2017; Barnes et al. 2017), a spin-off project of EAGLE consisting in a set of zoom-in hydrodynamical simulations of 30 galaxy clusters, having $\log(M_{200}/\mathrm{M}_\odot)$ ranging from 14.1 to 15.4 $\times$ 10^{14} $\mathrm{M}_\odot$ at $z = 0$. The clusters have been selected from the parent simulation, a dark-matter-only run of (3200 cMpc)^3 volume, to be isolated and not having another massive cluster in a radius of $20r_{200}$, and subsequently resimulated up to $10r_{200}$. The synthetic magnitudes in the SDSS bands have been calculated with the aid of the EMILES stellar library. Similarly to the observed clusters, we have computed the LFs of the galaxies as a function of redshift and we fit them using Schechter functions (see Negri et al., in preparation). Fig. 12 also shows the fitted parameters of the stacked and individual LFs of galaxy clusters from the Cluster-EAGLE cosmological simulation. In addition, these simulated clusters are located in the redshift interval $z = [0, 2]$, which allows us to follow the evolution of the LFs over $\sim$10 Gyr.

The stacked LFs of the simulated clusters show small changes in M_r^* and α from $z = 2$ to $z = 0$, and at $z = 0$ show M_r^* and α values close to the values of the stacked observed LFs (De Propris et al. 2002; Christlein & Zabludoff 2003). In contrast, the Moretti et al. (2015) stacked LF is flatter and shows a brighter M_r^* than the simulated clusters, partially due to the fact that this LF is not so deep as the other two surveys. Larger differences in M_r^* and α can be seen between simulations and individual clusters. The value of

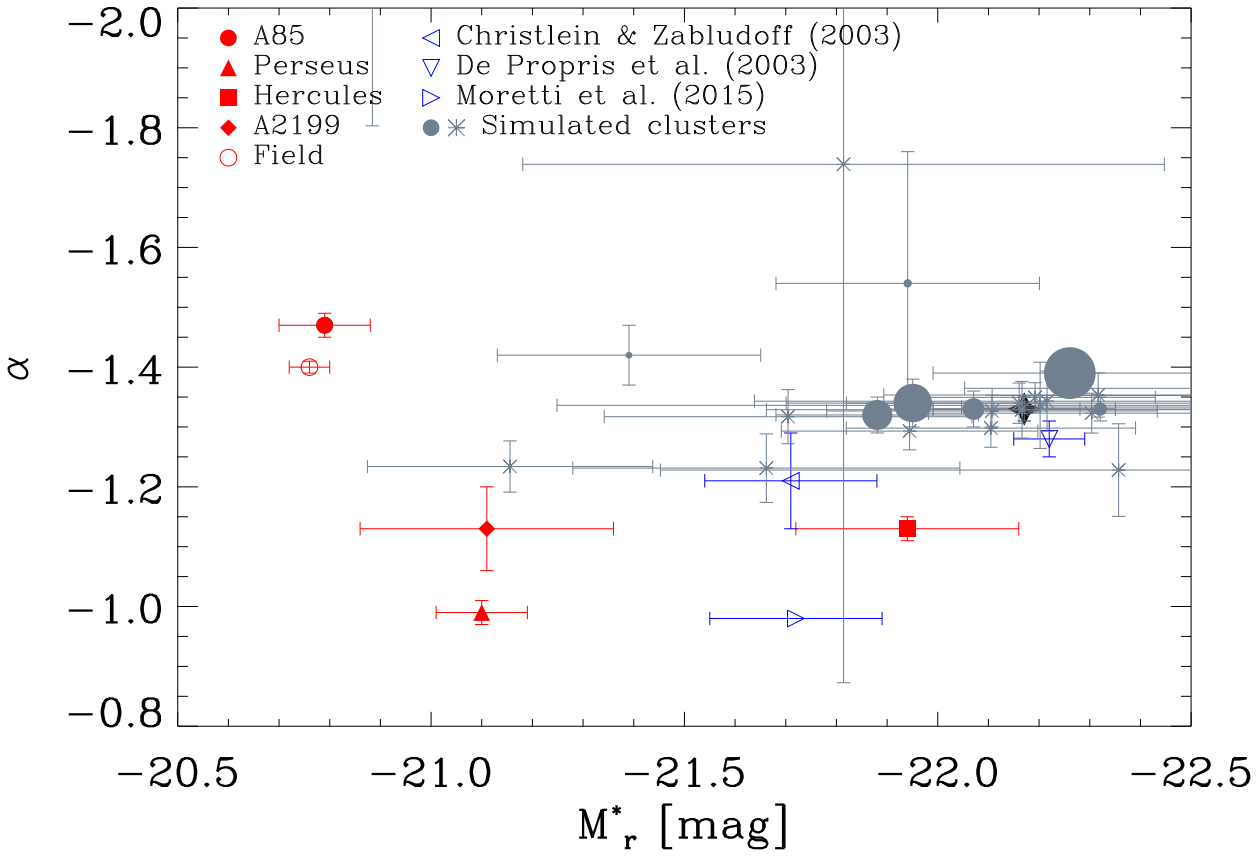

Figure 12. M_r^* and α parameters of the Schechter LFs of the clusters A 85 (red filled circle), Perseus (red triangle), Hercules (red square), and the field (red open circle). The grey filled circles show the parameters M_r^* and α for the stacked LFs from galaxy clusters from the EAGLE simulation. The size of these symbols is scaled with the redshift of the cluster. Larger symbols represent larger redshift of the cluster. The black star shows M_r^* and α of the stacked LF at $z = 0$ for the simulated clusters. The asterisks represent M_r^* and α values of the LFs of the individual simulated clusters.

M_r^* of the stacked LFs at $z = 0$ for the simulated clusters is similar to the value presented by A 2151. However, this cluster shows a flatter LF not in agreement with the α value shown by the stacked LF from simulated clusters. A 85, A 2199, and A 426 show values of M_r^* about 1–1.5 mag fainter than the stacked LF of simulated clusters at $z = 0$. The value of α for the simulated clusters does not change largely with redshift. Thus, clusters at $z = 2$ show values of $\alpha \sim -1.4$ as those at $z = 0$, similar to the faint-end slopes obtained for A 85 and the field LFs. In contrast, they are steeper than those reported for A 2151, A 429, and A 2199. The constancy of M_r^* and α with the redshift has also been reported in other cosmological simulations such as Millennium (see Gozaliasl et al. 2014). Note that C-EAGLE and Millennium simulations are very different, the former being a hydrodynamic cosmological simulation while the latter being collisionless and populated with galaxies with a semi-analytical model.

Fig. 12 also shows the values of M_r^* and α of the individual LFs of the simulated clusters. The values of α of the individual LFs are in the interval $[-1.25, -1.4]$. Only one EAGLE cluster shows an LF with $\alpha < -1.4$. However, the uncertainties for the LF parameters for this cluster are large. The values of M_r^* of the individual simulated clusters are in the interval -21.0 to -22.5. Only one cluster shows an M_r^* value of about -21.0. This cluster shows M_r^* values similar to those of A 2199 or A 426. In summary, Fig. 12 shows that simulated clusters at $z \sim 0$ do not present flat LF as those observed for A 2151, A 426, or A 2199. In addition, very few simulated clusters show M_r^* values similar to those of A 85, A 2199, or A 426. New deep spectroscopic surveys in the near future will report whether these differences between observations and simulations are statistically significant.

We have also compared the D/G ratio of the observed clusters (A 85, A 2151, A 426, and A 219) and those obtained from the cluster in the cosmological simulations. In all cases, except A 2199, the D/G ratios were computed within r_{200}. The D/G ratio of A 2199 was computed by using the LF given by Rines & Diaferio (2006), which is computed within $\sim 0.5 r_{200}$. This means that the D/G ratio obtained for this cluster should be taken as a lower limit. Fig. 13 shows the D/G ratio as a function of the cluster mass for A 85, A 2151, A 2199, and A 426. We have also included in this figure the D/G ratio obtained from the clusters in the numerical simulations. The cosmological clusters reproduce the D/G values of A 85, A 2151, and A 2199. Nevertheless, the D/G ratio of A 426 is smaller than that reported from the cosmological simulations for clusters with this mass.

4.4 Dependence of the LF parameters on cluster properties

Why do clusters show different LFs? Do the parameters of the cluster LFs depend on cluster properties? The answers to these questions are poorly understood and the previous analysis reported contradictory results. Zandivarez & Martínez (2011) show a clear dependence of the galaxy LF in clusters on the mass of the

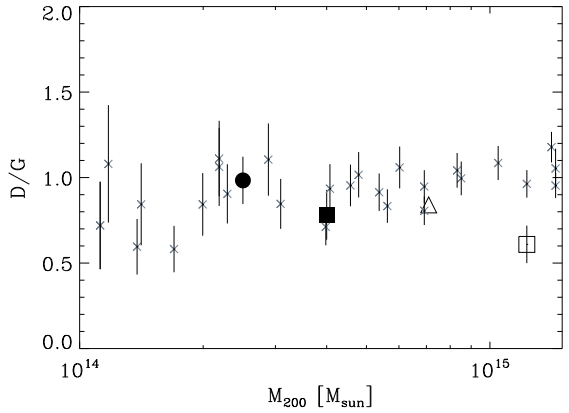

Figure 13. The D/G ratio as a function of the mass of the clusters for A 85 (filled circle), A 2151 (filled square), A 2199 (open triangle), and A 426 (open square). The crosses represent the D/G ratio of the clusters from cosmological simulations (see text for more details).

halo. Instead, Moretti et al. (2015) reported no dependence of the LF parameters on the properties of the clusters such as X-ray luminosity or velocity dispersion, both quantities related to their mass. Our sample of four clusters is small, but we can use them to find some hint of correlation that can be confirmed by using larger cluster samples in the future. We show here the dependence of M_r^* and α on the dominance of the brightest cluster galaxy (BCG). Simulations show that BCGs are the outcome of intense merging processes between galaxies. Therefore, the growth of the mass/luminosity of the BCGs could influence the galaxy population of the cluster. In particular, the dominance of the BGC in the cluster indicates the amount of stars in the clusters that are located within the BGC.

The dominance of the BCG can be studied by computing the parameter Δm_{12}, which is the magnitude difference between the two brightest galaxies of the cluster within some aperture. This dominance of the BCG can tell us about internal galaxy processes, like mergers, that happened in the cluster during its evolution. According to these parameters, galaxy clusters and groups are classified as fossil systems when having $\Delta m_{12} > 2.0$ (Ponman et al. 1994; D'Onghia et al. 2005; Aguerri et al. 2011; Zarattini et al. 2014) and non-fossil ones ($\Delta m_{12} < 2.0$). Fig. 14 shows the relations of the LF parameters and Δm_{12} for four nearby clusters with deep spectroscopic LF (A 85, A 426, A 2199, and A 2151). This figure shows a relation between M_r^* and Δm_{12} for these clusters. Thus, the cluster with the smallest Δm_{12} (the Hercules cluster) shows the brightest M_r^* value. In contrast, the cluster with the largest Δm_{12} (A 85) has the faintest M_r^*. There is also a relation between α and Δm_{12} (see Fig. 14). Thus, A 85 is the cluster with the steepest faint end and with the larger value of Δm_{12}. In contrast, Hercules, A 2199, and Perseus show small values of Δm_{12} and flatter LFs.

The dependence of M_r^* and α on Δm_{12} was analysed by Zarattini et al. (2015) for a sample of groups and cluster galaxies by using LFs combining photometric and spectroscopic data. The bright part of their LF was mainly spectroscopic. In contrast, the faint end of the LF is purely photometric (Zarattini et al. 2015). They observed that systems with larger Δm_{12} show fainter M_r^* and flatter faint end. We have found a qualitatively similar trend as shown in Fig. 14, where we compare our results with those of Zarattini et al. (2015). Note that the dependence of M_r^* on Δm_{12} is qualitatively similar between the two samples of clusters. This could be related to the fact that the central galaxies in clusters are formed by the

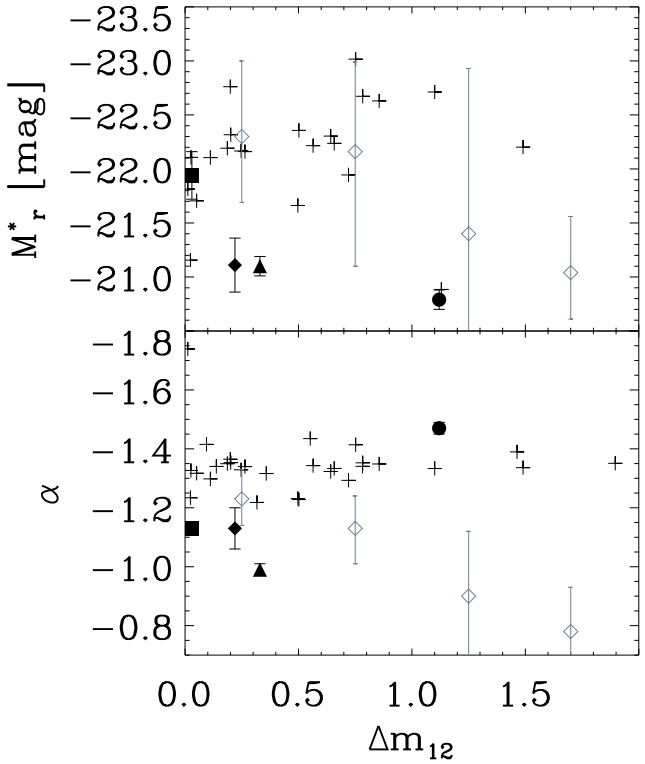

Figure 14. M_r^* and α parameters of the Schechter LFs as a function of Δm_{12} for the clusters A 85 (circle), Perseus (triangle), Hercules (square), and A 2199 (diamond). The grey diamonds show the data from Zarattini et al. (2015). The crosses show the values of M_r^* and α from the simulated clusters from EAGLE.

mergers of L^* nearby galaxies. This shows that as the mass of the BCG grows (or Δm_{12} grows), the number of bright galaxies in the clusters dismisses (or M^* becomes fainter). This intense merging process shows that BCGs in systems with larger magnitude gap are more massive or luminous (Kundert, D'Onghia & Aguerri 2017). In the α–Δm_{12} plot, A 85 strongly deviates from the Zarattini et al. (2015) relation. Since A 85 does not follow the typical relation between the two fitting parameters $M*$ and α in clusters as shown in Fig. 11 (see e.g. fig. 5 of Zarattini et al. 2015; fig. 6 of Barrena et al. 2012), the result for A 85 seems more likely related to some peculiarity of the cluster itself than to an inversion in the relation. More data from more clusters are needed to investigate this point. We also stress that the LFs from Zarattini et al. (2015) are purely photometric in its faint end. We have seen that there is a large difference between the faint end reported by photometric and spectroscopic LFs.

Fig. 14 also shows the values of M_r^* and α as a function of Δm_{12} for the EAGLE cluster. Note that simulated clusters show no dependence of the values of M_r^* and α on the dominance of the BCG. This means that in the simulated clusters there is no relation between the formation of the BCG and the satellite population contrary to what is reported by the observed clusters.

5 CONCLUSIONS

We have presented the results from a deep spectroscopic campaign conducted on the Perseus cluster. As a result, a total of 403 galaxies down to $M_r = -16.0$ resulted to be members of the Perseus cluster. This enlarges by a factor of 2 the number of cluster members

obtained so far in the literature. Using these members, we obtained the central velocity and velocity dispersion of the cluster (V_c = 5245 km s^{-1} and σ_c = 1040 km s^{-1}). Assuming an Navarro-Frenk-White (NFW) mass profile with $c = 5.1$, we have obtained that the mass of the cluster is $M_{200} = 1.23 \pm 2.5 \times 10^{15}$ M$_\odot$ and $r_{200} = 2.2$ Mpc.

The colour–magnitude diagram of the galaxies in the cluster was obtained down to the dwarf regime. The red sequence of the cluster is well defined for the bright galaxy population ($M_r < -19.0$). In contrast, it is not well formed for fainter galaxies. This indicates that the red dwarf population of the Perseus cluster is still forming at present. This is related to the fact that the velocity dispersion of the dwarf galaxies is larger than that for bright ones, indicating that this galaxy population is still not virialized.

The spectroscopic LF of the cluster was obtained using these new data. The fit of the LF was obtained by a Schechter function. We obtained a flat LF with $\alpha = 0.99 \pm 0.06$ with $M_r^* = 21.11 \pm 0.21$ as the best-fitting parameters. In addition, the number density of blue and red galaxies is similar at the faint end. The characteristic magnitude of the LF of the clusters turned to be $M_r^* = -21.11 \pm 0.21$. We have compared the parameters of the LF of the Perseus cluster with other nearby clusters with spectroscopic data in the literature. In particular, the LF of the Perseus cluster shows similar M_r^* to other systems such as A 2199 or A 85. In contrast, the Perseus cluster shows a flatter LF than other systems such as A 85, A 2199, or A 2151. We have also compared the observed spectroscopic LFs with those obtained from clusters in numerical simulations. In particular, cosmological simulations fail to reproduce the LF of those clusters with flat faint ends and/or faint M^*. New deep spectroscopic observations in large samples of nearby galaxy clusters are needed in order to confirm the statistical significance of the differences reported between simulated and observed clusters.

ACKNOWLEDGEMENTS

JALA and IA thank the support of this work by the Spanish Ministerio de Economia y Competitividad (MINECO) under the grant AYA2017-83204-P. This research had made use of SDSS Data Release 13 and the NASA/IPAC Extragalactic Database, which is operated by the Jet Propulsion Laboratory, California Institute of Technology, under contract with the National Aeronautics and Space Administration. The WHT and its service programme are operated on the island of La Palma by the Isaac Newton Group in the Spanish Observatorio del Roque de los Muchachos of the Instituto de Astrofísica de Canarias.

REFERENCES

Aguerri J. A. L., 2016, A&A, 587, A111
Aguerri J. A. L., González-García A. C., 2009, A&A, 494, 891
Aguerri J. A. L., Balcells M., Peletier R. F., 2001, A&A, 367, 428
Aguerri J. A. L., Iglesias-Paramo J., Vilchez J. M., Muñoz-Tuñón C., 2004, AJ, 127, 1344
Aguerri J. A. L., Gerhard O. E., Arnaboldi M., Napolitano N. R., Castro-Rodriguez N., Freeman K. C., 2005, AJ, 129, 2585
Aguerri J. A. L. et al., 2011, A&A, 527, A143
Aguerri J. A. L., Agulli I., Diaferio A., Dalla Vecchia C., 2017, MNRAS, 468, 364
Aguerri J. A. L., Agulli I., Méndez-Abreu J., 2018, MNRAS, 477, 1921
Agulli I., Aguerri J. A. L., Sánchez-Janssen R., Barrera R., Diaferio A., Serra A. L., Mendez-Abreu J., 2014, MNRAS, 444, L34
Agulli I., Aguerri J. A. L., Dominguez Palmero L., Diaferio A., 2016a, MNRAS, 461, L6
Agulli I., Aguerri J. A. L., Sánchez-Janssen R., Dalla Vecchia C., Diaferio A., Barrera R., Dominguez-Palmero L., Yu H., 2016b, MNRAS, 458, 1590
Agulli I., Aguerri J. A. L., Diaferio A., Dominguez Palmero L., Sánchez-Janssen R., 2017, MNRAS, 467, 4410
Ahn C. P. et al., 2014, ApJS, 211, 17
Andreon S., 1994, A&A, 284, 801
Arnaboldi M. et al., 2002, AJ, 123, 760
Bahé Y. M. et al., 2017, MNRAS, 470, 4186
Balogh M. L., Navarro J. F., Morris S. L., 2000, ApJ, 540, 113
Barkhouse W. A., Yee H. K. C., López-Cruz O., 2007, ApJ, 671, 1471
Barnes D. J. et al., 2017, MNRAS, 471, 1088
Barrena R., Girardi M., Boschin W., Mardirossian F., 2012, A&A, 540, A90
Benitez N. et al., 2014, preprint (arXiv:1403.5237)
Blanton M. R. et al., 2003, ApJ, 594, 186
Boselli A., Gavazzi G., 2014, A&AR, 22, 74
Castro-Rodriguéz N., Arnaboldi M., Aguerri J. A. L., Gerhard O., Okamura S., Yasuda N., Freeman K. C., 2009, A&A, 507, 621
Cenarro A. J. et al., 2019, A&A, 622, A176
Christlein D., Zabludoff A. I., 2003, ApJ, 591, 764
Dalton G. et al., 2012, in McLean I. S., Ramsay S. K., Takami H., eds, Proc. SPIE Conf. Ser. Vol. 8446, Ground-Based and Airborne Instrumentation for Astronomy IV. SPIE, Bellingham, p. 84460P
De Propris R. et al., 2002, MNRAS, 329, 87
Domínquez Palmero L. et al., 2014, in Ramsay S. K., McLean I. S., Takami H., eds, Proc. SPIE Conf. Ser. Vol. 9147, Ground-Based and Airborne Instrumentation for Astronomy V. SPIE, Bellingham, p. 914778
D'Onghia E., Sommer-Larsen J., Romeo A. D., Burkert A., Pedersen K., Portinari L., Rasmussen J., 2005, ApJ, 630, L109
Ettori S., Fabian A. C., White D. A., 1998, MNRAS, 300, 837
Fadda D., Girardi M., Giuricin G., Mardirossian F., Mezzetti M., 1996, ApJ, 473, 670
Fasano G. et al., 2006, A&A, 445, 805
Furusho T., Yamasaki N. Y., Ohashi T., Shibata R., Ezawa H., 2001, ApJ, 561, L165
Geha M., Guhathakurta P., van der Marel R. P., 2003, AJ, 126, 1794
Giovanelli R., Haynes M. P., 1985, AJ, 90, 2445
Girardi M., Giuricin G., Mardirossian F., Mezzetti M., Boschin W., 1998, ApJ, 505, 74
Girardi M. et al., 2015, A&A, 579, A4
Gozaliasl G., Khosroshahi H. G., Dariush A. A., Finoguenov A., Jassur D. M. Z., Molaeinezhad A., 2014, A&A, 571, A49
Gunn J. E., Gott J. R., III, 1972, ApJ, 176, 1
Haines C. P., Merluzzi P., Mercurio A., Gargiulo A., Krusanova N., Busarello G., La Barbera F., Capaccioli M., 2006, MNRAS, 371, 55
Hudson M. J., Lucey J. R., Smith R. J., Steel J., 1997, MNRAS, 291, 488
Iodice E. et al., 2016, ApJ, 820, 42
Ivezić Ž. et al., 2019, ApJ, 873, 111
Katgert P. et al., 1996, A&A, 310, 8
Kennicutt R. C. Jr., 1992, ApJS, 79, 255
Kundert A., D'Onghia E., Aguerri J. A. L., 2017, ApJ, 845, 45
Kurtz M. J., Mink D. J., Wyatt W. F., Fabricant D. G., Torres G., Kriss G. A., Tonry J. L., 1992, in Worrall D. M., Biemesderfer C., Barnes J., eds., ASP Conf. Ser. Vol. 25, Astronomical Data Analysis Software and Systems I. Astron. Soc. Pac., San Francisco, p. 432
Lan T.-W., Ménard B., Mo H., 2016, MNRAS, 459, 3998
Larson R. B., Tinsley B. M., Caldwell C. N., 1980, ApJ, 237, 692
Laureijs R. et al., 2011, preprint (arXiv:1110.3193)
Lisker T., Grebel E. K., Binggeli B., 2006a, AJ, 132, 497
Lisker T., Glatt K., Westera P., Grebel E. K., 2006b, AJ, 132, 2432
Lisker T., Grebel E. K., Binggeli B., Glatt K., 2007, ApJ, 660, 1186
Madgwick D. S. et al., 2002, MNRAS, 333, 133
Mastropietro C., Moore B., Mayer L., Debattista V. P. , Piffaretti R., Stadel J., 2005, MNRAS, 364, 607
Mihos J. C., Hernquist L., 1994, ApJ, 425, L13
Mihos J. C., Harding P., Feldmeier J., Morrison H., 2005, ApJ, 631, L41
Mobasher B. et al., 2003, ApJ, 587, 605
Mohr J. J., Fabricant D. G., Geller M. J., 1993, ApJ, 413, 492

Moore B., Lake G., Katz N., 1998, ApJ, 495, 139
Moretti A. et al., 2015, A&A, 581, A11
Munari E., Biviano A., Borgani S., Murante G., Fabjan D., 2013, MNRAS, 430, 2638
Oman K. A., Hudson M. J., Behroozi P. S., 2013, MNRAS, 431, 2307
Paccagnella A. et al., 2017, ApJ, 838, 148
Pedraz S., Gorgas J., Cardiel N., Sánchez-Blázquez P., Guzmán R., 2002, MNRAS, 332, L59
Peng Y., Maiolino R., Cochrane R., 2015, Nature, 521, 192
Phillipps S., Driver S. P., Couch W. J., Smith R. M., 1998, ApJ, 498, L119
Pisani A., 1993, MNRAS, 265, 706
Ponman T. J., Allan D. J., Jones L. R., Merrifield M., McHardy I. M., Lehto H. J., Luppino G. A., 1994, Nature, 369, 462
Popesso P., Biviano A., Böhringer H., Romaniello M., 2006, A&A, 445, 29
Postman M. et al., 2012, ApJS, 199, 25
Quilis V., Moore B., Bower R., 2000, Science, 288, 1617
Rines K., Diaferio A., 2006, AJ, 132, 1275
Sánchez-Janssen R., Aguerri J. A. L., Muñoz-Tuñón C., 2008, ApJ, 679, L77
Schaye J. et al., 2015, MNRAS, 446, 521
Schechter P., 1976, ApJ, 203, 297
Schwarz R. A., Edge A. C., Voges W., Boehringer H., Ebeling H., Briel U. G., 1992, A&A, 256, L11
Silk J., Mamon G. A., 2012, Res. Astron. Astrophys., 12, 917
Simionescu A. et al., 2011, Science, 331, 1576
Smith R. J., Lucey J. R., Hudson M. J., 2009, MNRAS, 400, 1690
Struble M. F., Rood H. J., 1999, ApJS, 125, 35
Toloba E. et al., 2009, ApJ, 707, L17
Toloba E. et al., 2015, ApJ, 799, 172
Treu T., Ellis R. S., Kneib J.-P., Dressler A., Smail I., Czoske O., Oemler A., Natarajan P., 2003, ApJ, 591, 53
Tully R. B., 1988, AJ, 96, 73
van de Voort F., Bahé Y. M., Bower R. G., Correa C. A., Crain R. A., Schaye J., Theuns T., 2017, MNRAS, 466, 3460
Wegner G., Haynes M. P., Giovanelli R., 1993, AJ, 105, 1251
Weinmann S. M., Lisker T., Guo Q., Meyer H. T., Janz J., 2011, MNRAS, 416, 1197
White S. D. M. et al., 2005, A&A, 444, 365
Wittmann C. et al., 2017, MNRAS, 470, 1512
Yu H., Diaferio A., Agulli I., Aguerri J. A. L., Tozzi P., 2016, ApJ, 831, 156
Zandivarez A., Martínez H. J., 2011, MNRAS, 415, 2553
Zarattini S. et al., 2014, A&A, 565, A116
Zarattini S. et al., 2015, A&A, 581, A16

This paper has been typeset from a TEX/LATEX file prepared by the author.